ROYAL SOCIETY OPEN SCIENCE

royalsocietypublishing.org/rsos

CC BY

Research

Cite this article: Chialina TM, Gentili HG, Pérez-Schuster V, Minoli SA, Beron de Astrada M. 2026 Ontogenetic changes in eye morphology and sensitivity are associated with wing development in kissing bugs. *R. Soc. Open Sci.* **13**: 261327.
https://doi.org/10.1098/rsos.261327

Received: 19 June 2026
Accepted: 8 October 2026

Subject Category:
Organismal and Evolutionary Biology

Subject Areas:
behaviour, ecology, neuroscience

Keywords:
insect vision, visual ecology, sensory biology, nocturnal vision, kissing bugs, triatominae, hemimetabolous insects, compound eye, post-embryonic development, visual behaviour

Authors for correspondence:
Martin Beron de Astrada
e-mail: martin@fbmc.fcen.uba.ar
Sebastián A. Minoli
e-mail: minoli@bg.fcen.uba.ar

Supplementary material is available online at https://doi.org/10.6084/m9.figshare.c.8784975.

THE ROYAL SOCIETY PUBLISHING

Ontogenetic changes in eye morphology and sensitivity are associated with wing development in kissing bugs

Tomás Manuel Chialina[1,2,6], Hernán Gustavo Gentili[1,3], Verónica Pérez-Schuster[1,4,6], Sebastián A. Minoli[2,5] and Martin Beron de Astrada[1,6]

[1]Departamento de Fisiología y Biología Molecular y Celular, Instituto de Biociencias, Biotecnología y Biología traslacional (iB3), Facultad de Ciencias Exactas y Naturales, [2]Departamento de Biodiversidad y Biología Experimental, Facultad de Ciencias Exactas y Naturales, [3]Departamento de Química Biológica, Facultad de Ciencias Exactas y Naturales, [4]Departamento de Física, Facultad de Ciencias Exactas y Naturales and [5]Instituto de Biodiversidad y Biología Experimental y Aplicada (IBBEA), CONICET–Universidad de Buenos Aires, Buenos Aires, Argentina
[6]Comisión Nacional de Investigaciones Científicas y Técnicas (CONICET), Buenos Aires, Argentina

MBdA, 0000-0003-1928-3808

Kissing bugs are the vectors of Chagas disease, one of the major endemic diseases in the Americas, now spreading to other continents. We used *Rhodnius prolixus* as a kissing-bug model species to characterize compound eye growth throughout the post-embryonic development of this hemimetabolous insect. We found that the adult eye is larger than expected from ontogeny. Moreover, while the eye grows symmetrically across nymphal instars, adults show greater ventral growth, resulting in a dorsoventrally asymmetrical eye. By studying a bright pseudopupil in natural mutant animals, we observed no major differences in spatial sampling frequency between the last nymphal instar and the adult stage. However, the adult eye possesses significantly larger ommatidia, particularly in the ventral region, shifting the area of highest sensitivity from the equatorial region in nymphs to the ventral region in adults. A similar growth pattern was observed in *Triatoma infestans* and *Panstrongylus megistus*. Analysis of photographic records from 39 species across 10 genera indicates that an asymmetrical eye is the predominant pattern in adult kissing bugs. Notable exceptions in species in which adults are wingless reveal a tight association between a large asymmetrical eye and the presence of wings, suggesting that vision may support dispersal and host-seeking flights.

© 2026 The Authors. Published by the Royal Society under the terms of the Creative Commons Attribution License http://creativecommons.org/licenses/by/4.0/, which permits unrestricted use, provided the original author and source are credited.

1. Introduction

Triatomines (Heteroptera: Reduviidae: Triatominae), commonly known as kissing bugs, constitute a subfamily of reduviid bugs whose principal diagnostic character is their obligatory haematophagy [1]. The post-embryonic development of kissing bugs consists of five sequential nymphal instars followed by an adult stage. Being hemimetabolous insects, the anatomical changes are quite gradual and progressive across stages, however, adults distinctively develop reproductive maturity, two pairs of exocrine thoracic glands, two pairs of wings and a pair of ocelli. Throughout their life cycle, kissing bugs are potential vectors of the parasite *Trypanosoma cruzi*, which they can transmit to their mammalian hosts, causing Chagas disease, a condition that affects millions of people across the Americas [2]. This is one of the main reasons that have motivated extensive studies of the ecology, physiology and behaviour of kissing bugs (e.g. [3]).

Over 150 species of triatomines, grouped into 17 extant genera [4], inhabit diverse wild and domestic microhabitats. These habitats range from vertebrate shelters (subterranean or arboreal), bird nests and human dwellings to cattle corrals and chicken coops. They also include spaces with no direct relationship to the hosts, such as rock outcrops, trees, palm crowns, various plants and epiphytes [5]. Kissing bugs may live and feed inside the nests or shelters of their vertebrate hosts, or they may actively search for and opportunistically feed on diverse hosts that temporarily share their microhabitat [6]. The activity of these insects is concentrated during crepuscular and nocturnal hours [7,8], matching their hosts' resting periods, which likely reflects a strong selective pressure to avoid host defensive behaviours [9,10]. Unlike nymphs, winged adults can disperse and actively search for hosts by flight, driven by hunger or by environmental factors such as ambient temperature [11].

Triatomines have not been considered highly visual insects. Studies on their visually-guided behaviours are rather scant compared to studies on other sensory modalities [3]. It was observed that several species avoid illuminated spaces guided by a marked negative phototaxis [12]. However, some triatomine species also show positive phototaxis to dim punctual light sources, as evidenced in both laboratory experiments and natural environments (e.g. [13]). In addition, reports of arrivals of flying triatomines to house lights are frequent in endemic areas [14]. While these phototactic behaviours are rather simple in their demands of visual system capabilities, visual behaviours that involve motion or object detection require more complex visual processing (e.g. [15]). In this respect, Lazzari & Varjú [16] found that *T. infestans* can fixate moving targets in the posterolateral region of their visual field. This would allow the animals to visually track a potential predator while still being able to escape in a direction away from it. More recently, Chialina *et al.* [17] found that *R. prolixus* consistently responds to moving visual threats by either freezing or directionally escaping, rapidly switching between these behaviours in an adaptive manner.

The visual system supporting spatial vision in reduviids, and particularly in triatomines, has been scarcely characterized (but see [18,19]). Triatomines possess a pair of rather globose compound eyes laterally protruding from their head capsule. These are apposition compound eyes in which the ommatidia possess open rhabdoms. The rhabdom is composed of a ring of six rhabdomeres (R1–6) surrounding a central pair of rhabdomeres (R7–8) [18,20]. The only two species of this group in which quantitative analyses of the eyes have been carried out, *Triatoma infestans* and *Rhodnius prolixus*, have been reported to possess between 30 and 400 ommatidia depending on the developmental stage [21]. These eyes exhibit features consistent with the ability to adapt to strong variations in ambient light intensity. For instance, it has been observed that screening pigments inside retinular cells and primary pigment cells form a dynamic 'pupil' in the ommatidia of *R. prolixus* and *T. infestans*, whose diameter varies with light intensity and time of day, respectively [18,22].

The epidemiological importance of triatomines, along with the complex visual behaviours they exhibit, motivated us to comprehensively characterize the morphology of their compound eyes. Using *R. prolixus* as a model species, we conducted a detailed study of the eye across its post-embryonic development. Here, we show that their eyes increase in size beyond expected by ontogeny and become asymmetrical when transitioning from the last nymphal instar to the adult stage. The eyes undergo a ventral expansion that shifts the region of greatest light sensitivity from the equatorial zone in nymphs to the ventral zone in adults. The analysis of photographic records from 39 species across 10 genera indicates that an asymmetrical eye is the predominant eye pattern in adult triatomines. Notably, in certain species in which some adults are apterous, this eye pattern is absent in wingless individuals, which strongly suggests that the compound eyes support flight in triatomines.

2. Material and Methods

2.1. Animals

R. prolixus (Stäl, 1859) was reared at the Bioterio de Animales No Tradicionales of the Facultad de Ciencias Exactas y Naturales (Universidad de Buenos Aires). All stages (egg, nymph with its five different instars and adult) were kept in a rearing chamber at 28 ± 1°C, 30–60% relative humidity with an inverted 12L:12D photoperiod (scotophase starting at 8.00 h and photophase at 20.00 h). Once a week, all individuals were fed ad libitum on live hens (handled according to the biosafety rules from the Servicio de Higiene y Seguridad of the university) and grouped according to their developmental stage. All individuals used in this work were aged at least 7 days post-ecdysis. Both females and males were included in this work, but, as no differences were found between them, we have grouped them with no gender specification along the article.

Wild-type (black-eyed) individuals were used to study eye growth (figures 1 and 2). Instead, red-eyed mutant animals were used to study visual fields, sampling frequency and optical sensitivity (figures 3 and 4). These mutants were chosen because of the advantages they possess for pseudopupil imaging (§2.3).

2.2. Morphometrics of compound eyes

2.2.1. Morphometric measurements

To assess eye growth along the anteroposterior (AP) extent of the eye, images of the entire head in dorsal view of the five nymphal instars and the adult stage were taken to measure: head length (HL), total eye perimeter (EP^{AP}) and eye anterior and posterior perimeters (EP^{Ant} and EP^{Post}, respectively). To account for growth along the dorsoventral (DV) extent of the head, head cross-sections were obtained after washing the sample in 96% ethanol for several minutes to soften the cuticle [23]. Then, we performed a clean transverse cut through the middle of the eyes. Head cross-sections were obtained only for the last three nymphal instars and the adult stage, because in smaller instars we had difficulty cutting the heads without distorting the eyes. The images of these sections were then used to measure: head perimeter (HP), total eye perimeter (EP^{DV}) and eye dorsal and ventral perimeters (EP^{Dor} and EP^{Ven}, respectively). Images of heads in dorsal view and head cross-sections were acquired with a color CMOS camera attached to a stereomicroscope (SZX10, Olympus Corporation, Japan). Image analyses were conducted using FIJI [24].

Head dimensions were chosen to estimate body size throughout development, rather than other body dimensions, because head measurements exhibit less variability than those including the extensible abdomen length [23]. Our measurement of HL spanned from the posterior margin of the cervix (at the junction with the prothorax) to the base of the rostrum (figure 2*A*). As *R. prolixus* head has a cylindrical section, the HP in cross-section was simply estimated by fitting a circle that included both the dorsal and ventral region of the head not occupied by the eyes (figure 2*C*).

To count the total number of ommatidia in the compound eye across stages, we generated three-dimensional (3D) representations of the eyes based on Z-stacks acquired with a confocal microscope (LSM 980, ZEISS, Germany). Taking advantage of the autofluorescence of the cuticle of these insects, images were acquired at an emission wavelength of 509 nm after exciting the sample with a 488 nm laser. For each reconstructed eye, we additionally selected a set of 4 to 6 ommatidia from the lateral region at the eye's equator to quantify their diameters. To do so, a circle was fitted to the facet contour.

2.2.2. Data analysis

Statistical analyses were conducted in the R environment (version 4.3.1). General linear models were fitted using the nymphal instar as a continuous explanatory variable. The individual identity was used as a random effect in the cases where multiple measurements were taken from the same insect (i.e. DV and AP eye perimeters and facet diameters). For each response variable, linear regressions in both natural and logarithmic scale were performed [23]. The better of these two fits was chosen based on the Akaike information criterion. Regression slope estimates and significance levels are reported in table S1 in the supplementary material. A one-sample *t*-test was performed to determine if the adult observed mean value was significantly different from the adult mean predicted by the nymphal regression model [23].

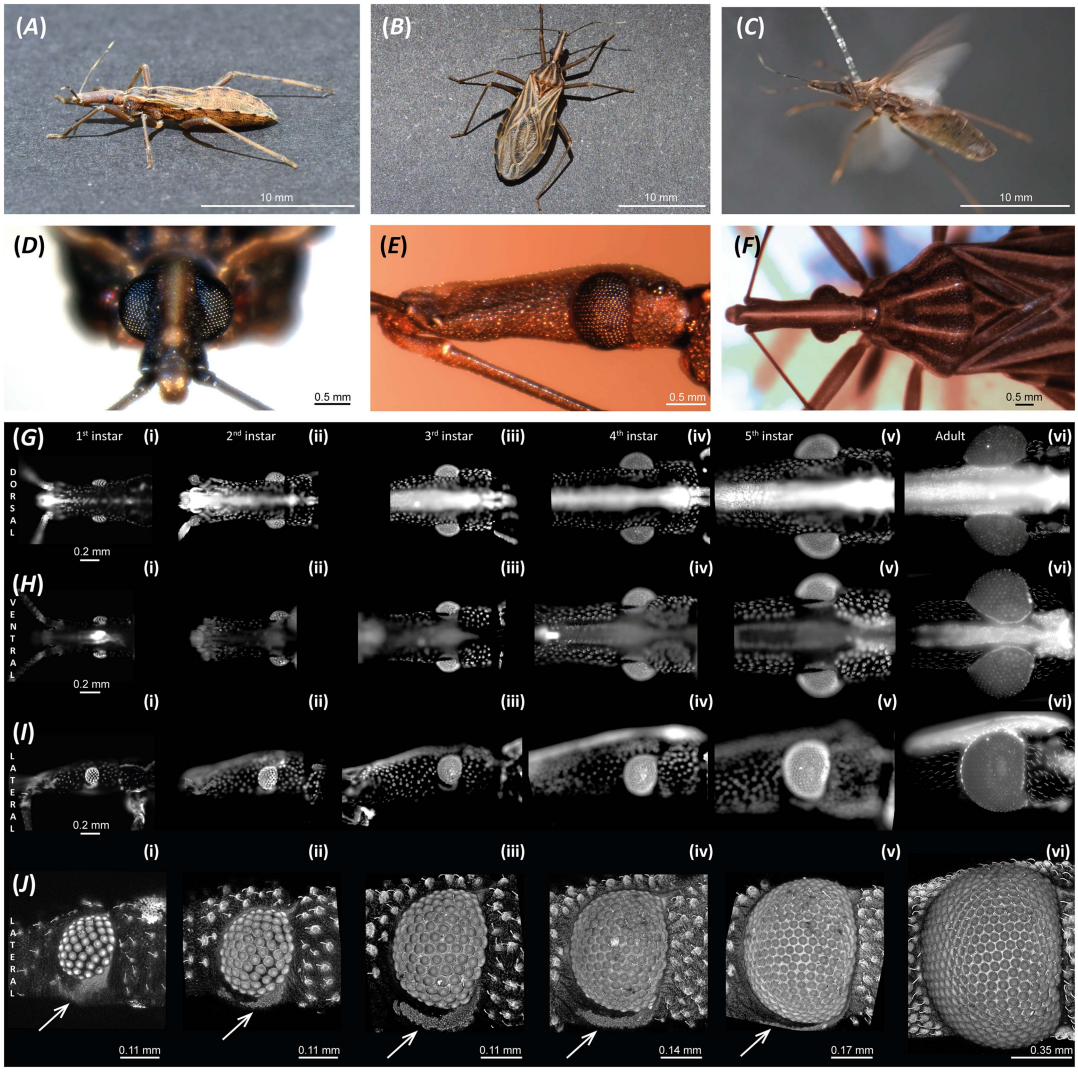

Figure 1. General morphology and post-embryonic growth of the compound eye in *R. prolixus*. (*A*) Fifth-instar nymph in walking posture. (*B–C*) Images illustrating the locomotion modes of an adult: walking and flight, respectively. (*D*) Frontal, (*E*) lateral and (*F*) dorsal views of the head of an adult. (*G*) Dorsal, (*H*) ventral and (*I*) lateral views of the head across all developmental stages under an epifluorescence microscope (§2.3.2), respectively. This optical method was preferred because the autofluorescence of the cuticle of these insects yields excellent contrast of the compound eyes. (*J*) Confocal microscopy images of the compound eyes in lateral view for all stages. Each image consists of a Z-projection of a compound eye. For panels (*G*)–(*J*), (i)–(v) represent the nymphal instars (I–V), and (vi) represents the adult stage. Arrows indicate a bright curved band ventral to the compound eye, present only in nymphal instars. Scale bars in panels (*G*)–(*I*) apply to all images (i–vi) within each respective row.

When multiple measurements were obtained per adult insect, an individual mean was calculated for each insect to prevent pseudoreplication in the *t*-tests. Test statistics (t) and degrees of freedom (d.f.) for the *t*-tests are reported in table S2 in the supplementary material. In all cases, a level of significance of 0.05 was used. If no significant differences were found in the *t*-test, the observed values for the adult stage were then included in the regression analysis.

2.3. Functional morphology

To characterize the visual field, spatial sampling frequency and optical sensitivity of the compound eye of fifth-instar nymphs and adults of *R. prolixus*, we imaged the eye pseudopupil, which allowed us to determine the optical axes of the ommatidia and measure their facet diameters [25]. We conducted these optical characterizations using red-eyed mutants, as they enable bright (autofluorescent) pseudopupil visualization under continuous illumination without light adaptation owing to their lack of pupillary

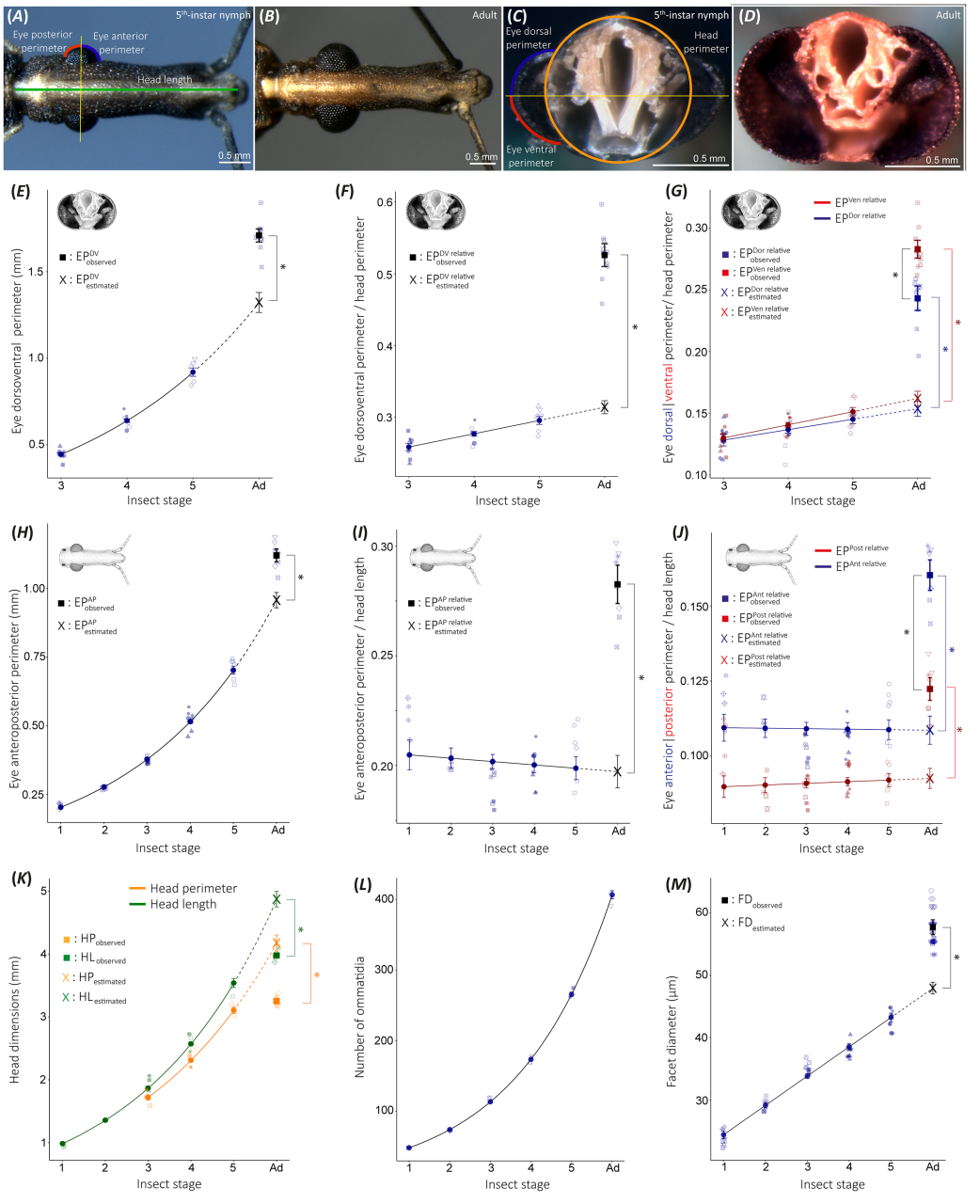

Figure 2. Quantification of eye growth of *R. prolixus*. (*A*,*B*) Dorsal views of the heads of a fifth-instar nymph and an adult, respectively. (*C*,*D*) Cross-sections of the heads of a fifth-instar nymph and an adult, respectively. Panels (*A*) and (*C*) also illustrate the measurements performed in each view. (*E*,*F*) Post-embryonic growth of the eye DV perimeter, expressed both in absolute terms (EP^{DV}) and relative to HP ($EP^{DV\ relative}$), respectively. (*G*) Dorsal (blue) and ventral (red) eye perimeters relative to HP ($EP^{Dor\ relative}$, $EP^{Ven\ relative}$) across stages. (*H*,*I*) Post-embryonic growth of the eye AP perimeter, expressed both in absolute terms (EP^{AP}) and relative to HL ($EP^{AP\ relative}$), respectively. (*J*) Anterior (blue) and posterior (red) eye perimeters relative to head length ($EP^{Ant\ relative}$, $EP^{Post\ relative}$) across stages. (*K*) HP and HL across stages. (*L*,*M*) Number and facet diameter of ommatidia across stages, respectively. Sample sizes: (*E–M*): $n = 2–5$ per stage, more statistical details in table S1. In (*E–M*), solid lines represent the results of the regression analyses, performed either in logarithmic (panels *E*,*H*,*K*,*L*) or natural (panels *F*,*G*,*I*,*J*,*M*) scale. Regression slope estimates and significance levels are reported in table S1. Insect stage was used as a numerical variable in the regression analyses shown, including the adult stage as the sixth stage. Filled circular markers with error bars represent the mean values estimated by the regression models, while semi-transparent markers show individual data points for each insect. Individual identity is coded by the specific combination of shape and fill in the semi-transparent markers. Filled square markers with error bars represent observed mean values for the adult stage, while crosses represent the estimated mean values for the adult stage based on an extrapolation of the growth trend of the nymphal instars. In all cases, error bars denote standard errors. Asterisks represent significant differences (p-value < 0.05) between estimated and observed values of the adult stage. When two eye perimeters were plotted in the same figure, a paired t-test was also performed to assess differences between the observed values of the adult for both perimeters (i.e. dorsal versus ventral, anterior versus posterior). In this cases, if differences were significant, a black asterisk was also added. Test statistics (t) and degrees of freedom (d.f.) for the t-tests are reported in table S2 in the supplementary material.

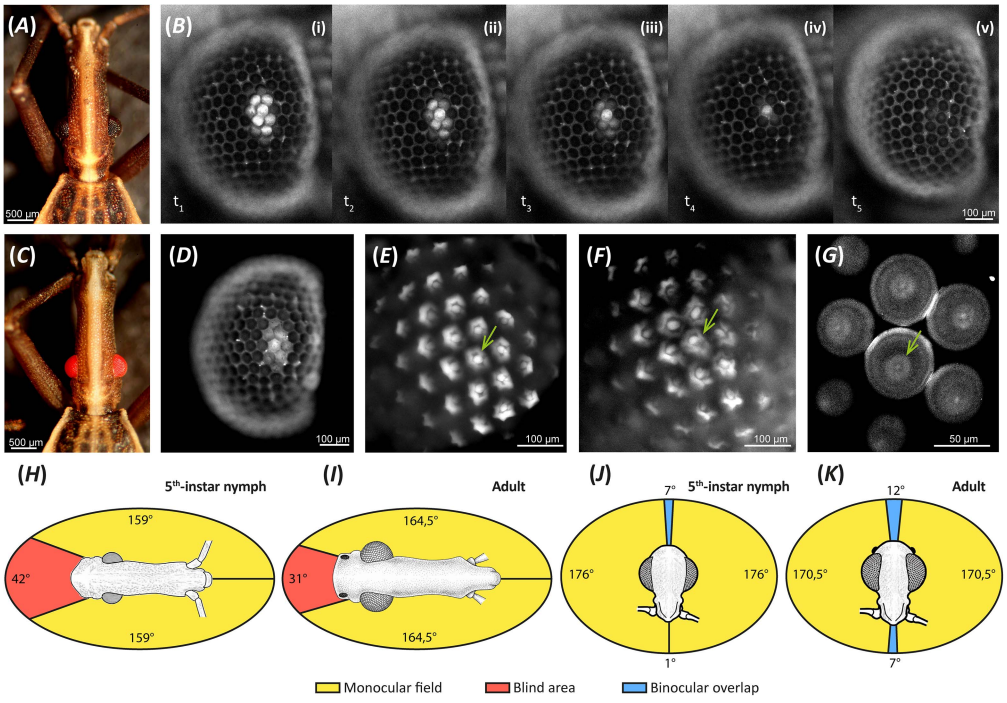

Figure 3. Autofluorescent pseudopupil and visual field of *R. prolixus*. (*A*,*C*) Dorsal view of a black-eyed (wild-type) and a red-eyed (mutant) fifth-instar nymph, respectively. (*B*) Time-lapse sequence (t1 = 0 s; t2 = 20 s; t3 = 52 s; t4 = 71 s; t5 = 120 s) of a dark-pigmented eye showing the gradual fading of the pseudopupil in response to continuous focal illumination under an epifluorescence microscope. (*D*) Lateral view of a red-pigmented compound eye, showing a constantly bright pseudopupil (no fading). (*E*,*F*) Open rhabdoms in *R. prolixus* dark-pigmented and red-pigmented compound eyes, respectively, revealed via epifluorescence microscopy with water immersion. (*G*) Open rhabdoms revealed by confocal microscopy. (*H*,*I*) Anteroposterior visual field of a fifth-instar nymph and an adult, respectively ($n = 2$ per instar). (*J*,*K*) Dorsoventral visual field of a fifth-instar nymph and an adult, respectively ($n = 2$ per instar). Green arrows in panels (*E*–*G*) indicate the position of an open-rhabdom, with its outer ring composed of photoreceptors R1–6 and its central pair of photoreceptors R7 and R8. Scale bar in panel (*B*) applies to all images (i–v) in the row.

screening pigments [19]. Interommatidial angles and facet diameters were quantified along two eye transects (figure 4): a horizontal (AP) transect traversing the eye equator and a vertical (DV) transect traversing the lateral visual field.

2.3.1. Eye preparation

The head of either a fifth-instar nymph or an adult was severed and sealed with beeswax to prevent desiccation. The antennae and the proboscis were immobilized to ensure unobstructed optical access to the eye. The head was then mounted onto a graphite stick using beeswax: if the eye transect to study was vertical, the stick was attached to the posterior end of the head, parallel to the longitudinal head axis; otherwise, if it was the horizontal transect, the stick was fixed proximally to the antennae, perpendicular to the longitudinal head axis.

In order to increase the contrast of the bright pseudopupil in some individuals, a fluorescent dye was injected to the animal prior to head excision, following a modified version of the protocol designed by Gutierrez *et al.* [26]. Briefly, the animal was immobilized on a slide with double-sided tape. A syringe with an angle of 30° with the long axis of the bug was inserted in the meso-thorax, and a constant pressure to the syringe plunge allowed a constant flux of a total 15–20 µl of a dye solution, which ended after a few minutes. The haemolymph flow through the dorsal vessel of the bug was sufficient to carry the dye to the cephalic capsule, thus bathing the optic lobes and the retina. After 30 minutes, the increase in fluorescence of the pseudopupil was notorious. The dye used was a purified TAT-GFP fusion protein dissolved in PBS buffer (0.80 mg ml^{-1}), but the technique worked with Lucifer Yellow as well.

Once the head was mounted, the graphite stick was placed inside a 3D-printed holder fitted over the shaft of a wireless rotary encoder (PS-3220, PASCO Scientific, Roseville, USA). The encoder wheel was coupled to a stepper motor (28BYJ-48, People's Republic of China). This custom-built goniometer was

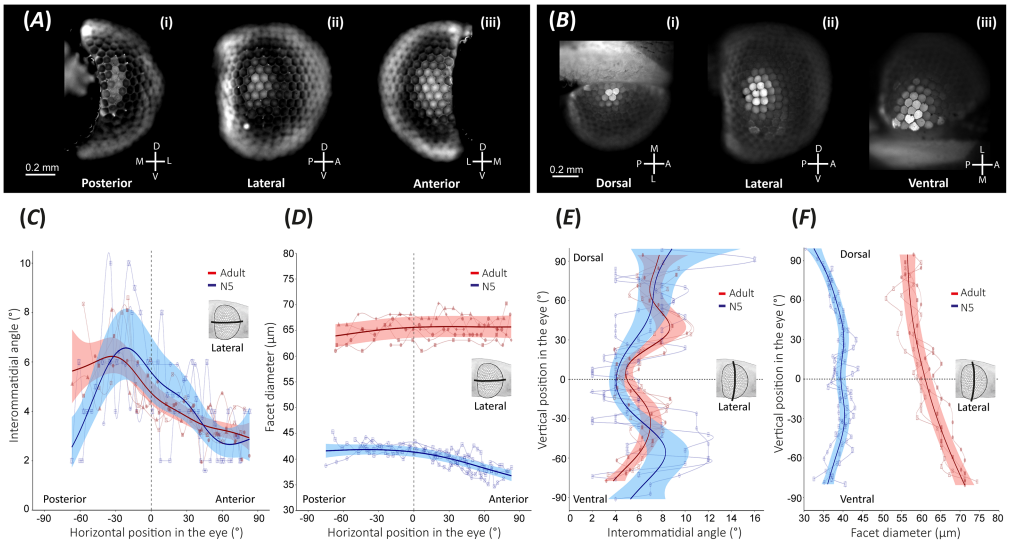

Figure 4. Spatial sampling frequency and optical sensitivity of the *R. prolixus* compound eye. (*A*,*B*) Views of the fluorescent pseudopupil at different regions along the horizontal (AP) and vertical (DV) transects of the eye, respectively: (i) posterior/dorsal; (ii) lateral; (iii) anterior/ventral. (*C–F*) Interommatidial angles and facet diameters along the horizontal and vertical transects of the eye for the fifth-instar nymph (blue) and the adult stage (red). Solid lines with shaded bands represent mean values with 95% confidence intervals. The curves result from fitting GAMMs to the data from all eyes measured for each stage. Thin solid lines represent individual traces of each eye analysed, and result from applying a monotone Hermite spline interpolation (following the method of Fritsch and Carlson) to data of each individual eye, for illustrative purposes only. Semi-transparent markers show data points at different angular positions in the transect for each individual eye. Eye identity is coded by the specific combination of shape and fill in the semi-transparent markers. Anatomical axes are shown in panels (*A*) and (*B*) for head orientations (D: dorsal; V: ventral; M: medial; L: lateral; A: anterior; P: posterior). Illustrations of the eye in lateral view in (*C–F*) indicate the locations of the transects sampled in the eye. All photographs have the same magnification.

controlled by an Arduino Uno board. The angular position of the encoder (and thus, of the eye) could be easily set with a custom Python script by specifying either step-wise 2° rotations or specific absolute angular positions.

2.3.2. Image acquisition

Images of the pseudopupil were captured using an epifluorescence microscope (BX51WI, Olympus Corporation, Japan). The system was equipped with a 10X objective (NA 0.20) and a filter set consisting of a 525 nm dichroic filter, a 470–490 nm band-pass excitation filter and a long-pass 530 nm emission filter. The LED light source (peak wavelength: 470 nm) was coaxially aligned with the imaging pathway of a CMOS camera (C11440, Hamamatsu Photonics, Japan). The filter arrangement is suited for imaging both autofluorescent and GFP-induced pseudopupils of *R. prolixus* (figures 3 and 4).

The eye was rotated in discrete 2° steps, spanning the full length of the analyzed transects. At each step, an image of the pseudopupil was captured. At both extremes of the eye, the process ended when the pseudopupil was no longer visible.

2.3.3. Pseudopupil mapping

The traditional pseudopupil mapping method [25–27] was used to estimate the angular separation between the optical axes of neighbouring ommatidia. This interommatidial angle sets the higher limit to the optical acuity of a compound eye [28]. Local interommatidial angles were obtained by measuring the shift of the pseudopupil centre (i.e. the number of ommatidial rows that it moves across) for a known rotation of the eye. Typically, the optical axis of the ommatidium at the pseudopupil centre was determined by identifying the angular position where its brightness was maximal. Additionally, we measured the facet diameters of the ommatidia whose optical axes had been determined, as a proxy of their optical sensitivity [25]. For the DV and AP transects, the angular reference (0°) was the angular position where the head was precisely aligned in dorsal or anterior view, respectively.

Finally, in an independent group of animals (two fifth-instar nymphs and two adults), we determined the visual fields of the right and left compound eyes and assessed the binocular overlap in the frontal, rear, dorsal and ventral regions. To this end, for each eye of an animal at each of these regions, we identified the maximum angular position where the pseudopupil was fully visible and distinguishable from the fluorescence of non-aligned ommatidia. The mean angular extent of each eye visual field was then calculated for each developmental stage.

2.3.4. Data analysis

Statistical analyses were also conducted in the R environment (version 4.3.1). Generalized additive mixed models (GAMM) were fitted to describe the variations of interommatidial angles and facet diameters as functions of the eye angular position along the two chosen transects. A gamma distribution was assumed for the response variables. We performed four independent GAMMs, one for each combination of transect (vertical/horizontal) and stage (nymph/adult). Angular position was included as a fixed effect, while the identity of the compound eye was specified as a random effect. For adult-stage GAMMs, individual identity was also included as a random effect since both eyes were sampled in some individuals. GAMMs were fitted using the mgcv package and model assumptions were evaluated using the DHARMa package.

3. Results

3.1. Eye growth morphometrics

In many different species, vision serves as a key sensory input for guiding locomotor behaviours such as walking or flying. Like most hemimetabolous insects, *R. prolixus* relies on walking locomotion throughout all developmental stages, whereas flight is acquired only at the adult stage (figure 1*A–C*). Its compound eyes are positioned laterally, presenting an approximately hemispherical shape protruding from the head. As in triatomines in general, the head of *R. prolixus* is elongated along the anteroposterior axis. Consequently, the anterior and posterior regions of the head constitute a steric impediment to vision. The lateral protrusion of the compound eyes, therefore, provides an expanded azimuthal visual field, particularly towards the anterior region (figure 1*D–F*).

Figure 1*G–I* displays the dorsal, ventral and lateral views of *R. prolixus* head across stages. A cursory inspection of the images reveals that the eyes grow with head size, always with the characteristic lateral protrusion. However, there is a considerable shift in eye size in the adult stage, where the eye grows considerably more relative to head size compared to the nymphal instars (figure 1*G*(vi)–*I*(vi) and 2). The size increment is more pronounced along the dorsoventral extent of the eye, significantly reducing the interocular distance in the dorsal and ventral regions of the head (figure 1*G*(vi)–*H*(vi)), though the change is larger in the latter (figure 1*H*(vi)). Notably, a distinct bright curved band is consistently observed on the dark cuticle ventral to the compound eye across all nymphal instars, occupying a constant position relative to the head (arrows in figure 1*J*(i–v)). This curved band is absent in the adult stage as the corresponding cuticular area is occupied by the eye (figure 1*J*(vi)).

We performed a quantitative analysis of eye size across stages for its anteroposterior (AP) and dorsoventral (DV) extents (figure 2*A–D*). This analysis reveals that the eye dorsoventral perimeter (EP^{DV}) in the adult stage is significantly larger than expected if we assume an exponential growth of this trait throughout stages (figure 2*E*; adult $EP^{DV}_{observed} = 1.71 \pm 0.04$ mm, adult $EP^{DV}_{estimated} = 1.32 \pm 0.06$ mm, *t*-test: $p < 0.001$, see tables S1 and S2 in the supplementary material for more statistical details). Notably, a deviation from the growth trend in the adult stage also occurs for head perimeter (HP), but with opposite sign: while eye perimeter accelerates its growth rate in the last stage, head perimeter decelerates its own, resulting in a smaller head perimeter than expected for the adult (figure 2K; adult $HP_{observed} = 3.25 \pm 0.04$ mm, adult $HP_{estimated} = 4.2 \pm 0.1$ mm, *t*-test: $p < 0.001$). For this reason, eye perimeter relative to head perimeter has a more dramatic change between expected and observed values in this last stage (figure 2F; adult $EP^{DV\ relative}_{observed} = 0.53 \pm 0.02$, adult $EP^{DV\ relative}_{estimated} = 0.314 \pm 0.009$, *t*-test: $p < 0.001$).

In addition, we separately analysed the development of the eye dorsal and ventral perimeters relative to the head perimeter (figure 2*G*). This analysis shows that the deviation from the growth trend in the adult stage is significant for both eye perimeters (figure 2*G*; adult $EP^{Dor\ relative}_{observed} = 0.24 \pm 0.01$, adult $EP^{Dor\ relative}_{estimated} = 0.154 \pm 0.006$; *t*-test: $p^{Dor} < 0.001$, blue asterisk; adult $EP^{Ven\ relative}_{observed} = 0.283 \pm 0.007$, adult

$EP^{Ven\ relative}_{estimated} = 0.162 \pm 0.006$; *t*-test: $p^{Ven} < 0.001$, red asterisk). Finally, we observed that, across nymphal instars, there are no differences between the ventral and dorsal perimeters ($GLMM^{Dor\text{-}vs\text{-}Ven}$ post hoc contrast: nymph $EP^{Dor\ relative}$ − nymph $EP^{Ven\ relative} = -0.003 \pm 0.003$, $p = 0.2$); whereas in the adult, the ventral perimeter is larger than the dorsal one resulting in an asymmetrical eye (*t*-test: $p = 0.004$, black asterisk).

With respect to the anteroposterior perimeter of the eye (EP^{AP}), a shift in the development trend of the eye is also evident at the adult stage. If we assume an exponential growth throughout stages, the eye perimeter observed for the adult is significantly larger than expected (figure 2*H*; adult $EP^{AP}_{observed} = 1.12 \pm 0.02$ mm, adult $EP^{AP}_{estimated} = 0.96 \pm 0.03$ mm, *t*-test: $p = 0.005$). The growth trend of head length (HL) also shows a deviation for the adult stage, but in the opposite direction: the observed value for the adult is significantly smaller than expected (figure 2*K*; adult $HL_{observed} = 3.98 \pm 0.04$ mm, adult $HL_{estimated} = 4.9 \pm 0.1$ mm, *t*-test: $p < 0.001$). Because of this, the deviation in the growth trend is much greater between expected and observed values for eye perimeter relative to head length (figure 2*I*; adult $EP^{AP\ relative}_{observed} = 0.283 \pm 0.009$, adult $EP^{AP\ relative}_{estimated} = 0.197 \pm 0.0\ 07$, *t*-test: $p = 0.002$).

Additionally, we separately analysed the development of the eye anterior and posterior perimeters relative to the head length. This analysis shows that the deviation from the growth trend in the adult stage is significant for both perimeters of the eye (figure 2*J*; adult $EP^{Ant\ relative}_{observed} = 0.160 \pm 0.005$, adult $EP^{Ant\ relative}_{estimated} = 0.109 \pm 0.005$; $p^{Ant} = 0.002$, blue asterisk; adult $EP^{Post\ relative}_{observed} = 0.122 \pm 0.004$, adult $EP^{Post\ relative}_{estimated} = 0.093 \pm 0.003$; *t*-test: $p^{Post} = 0.004$, red asterisk). Finally, we observed that the anterior region of the eye is larger than the posterior one in both nymphal ($GLMM^{Ant\text{-}vs\text{-}Post}$ post hoc contrast: nymph $EP^{Ant\ relative}$ − nymph $EP^{Post\ relative} = 0.015 \pm 0.001$, $p < 0.001$) and adult stages (*t*-test: $p < 0.001$, black asterisk).

The analysis of the number of ommatidia along ontogeny revealed an exponential growth for this trait throughout all the developmental stages, i.e. no deviation was observed for the adult in this case (figure 2*L*). However, a trend deviation in the adult stage was observed for the growth of facet diameter (FD) across stages (figure 2*M*; adult $FD_{observed} = 57.7 \pm 1.2$ µm, adult $FD_{estimated} = 47.9 \pm 0.9$ µm, *t*-test: $p = 0.001$).

Given that the main differences in eye growth in *R. prolixus* were found between the last (fifth) nymphal instar and the adult stage, the following analyses focused exclusively on these two stages.

3.2. Fluorescent pseudopupil

The most traditional method for describing the functional morphology of compound eyes involves mapping the principal pseudopupil, which reveals the ommatidial optical axes [25]. A bright pseudopupil can be revealed in dark-pigmented eyes of wild-type *R. prolixus* owing to photoreceptor fluorescence (figure 3*A–B*) [29]. However, this phenomenon is visible only for a very brief period of time owing to a light-adaptation process that involves the displacement of screening pigments (figure 3B(i–v)) [18,22]. For this reason, here, we used red-eyed mutants, which do not possess the screening pigments involved in this mechanism (figure 3*C*) [19]. Thus, we could illuminate the eye for prolonged periods of time without any significant decrease in fluorescence making them suitable for imaging the pseudopupil (figure 3*D*). Additionally, in some preparations, we intensified this fluorescence by injecting a fluorescent marker in the thorax of the animal to increase the contrast of the pseudopupil [26].

We have confirmed that in both eye phenotypes, the structures responsible for the autofluorescence phenomenon are the photoreceptors. In figure 3E-G (green arrows), the open rhabdoms typical of the heteropteran compound eye can be visualized [20]. The structure and shape of the open rhabdom seem to be well preserved in both the dark-eyed (figure 3*E*) and red-eyed insects (figure 3*F*). Additionally, we studied the visual defensive responses evoked in animals of both eye phenotypes when presented with a moving visual threat (supplementary material, figure S1). We found no differences between the responses of the two groups, suggesting that visual processing and sensitivity are not affected in red-eyed mutants. All these observations support the use of red-eyed mutants to study the functional morphology of the *R. prolixus* eye, as they indicate both structural and functional integrity.

3.3. Visual field

We determined the visual field of *R. prolixus* eyes by mapping the pseudopupil in the margins of the left and right eye in both the anteroposterior (horizontal) and dorsoventral (vertical) directions. Both fifth-instar nymphs and adults exhibit no binocular overlap in the horizontal plane, in either the frontal or the rear visual fields (figure 3*H*,*I*). While the frontal visual field is fully sampled in both stages,

the posterior field is partially captured. The blind area corresponds approximately to the area occluded by the animal's own body. The overall visual field in the horizontal plane is similar in both stages, spanning 318° and 329° for the fifth-instar nymph and the adult, respectively. By contrast, the vertical visual field extends across a full 360° range and exhibits slight dorsal and ventral overlap in both stages (figure 3*J*,*K*). These overlaps are slightly larger in the adult than in the nymph (dorsal overlap: nymph = 7°, adult = 12°; ventral overlap: nymph = 1°; adult = 7°).

3.4. Spatial sampling frequency and optical sensitivity

The interommatidial angles were determined by identifying the optical axes of the ommatidia through pseudopupil mapping along a horizontal and a vertical transect of the eye. Different shapes and sizes of the fluorescent pseudopupil in three angular positions along these two transects in an adult eye are shown in figure 4*A*,*B*. A larger pseudopupil implies smaller interommatidial angles and, consequently, greater spatial sampling frequency in that region of the eye. This is evident in the horizontal transect when comparing the pseudopupil horizontal dimension in the posterior (figure 4*A*(i)) and anterior regions of the eye (figure 4*A*(iii)): the latter exhibits a pseudopupil that recruits more ommatidia than the former (i.e. the latter possesses smaller interommatidial angles and thus higher sampling frequency). A quantitative analysis along the horizontal transect shows that, for both stages, interommatidial angles decrease similarly towards the anterior region of the eye. The maximum sampling frequency [28] in the frontal visual field is approximately 2.3 times higher than the minimum sampling frequency in the posterolateral visual field (figure 4*C*). By contrast, facet diameters show a large increase in the adult with respect to the nymph (figure 4*D*). The average facet size in the adult (65.3 ± 0.5 µm) increases 62% relative to the nymph (40.4 ± 1.6 µm), which implies a significant increase in the eye optical sensitivity.

Along the vertical transect of the eye, variations in the interommatidial angles were less smooth than along the horizontal transect (figure 4*E*). For both stages, we found large interommatidial angles in the dorsal region of the eye, a local minimum at the eye equator and small angles towards the ventral region of the eye. Only in the ventral-most region of the eye did we observe a slight reduction in the interommatidial angles of the adult eye relative to the nymphal eye. The facet diameters were consistently larger in the adult compared to the nymph along the entire transect (figure 4*F*). As observed in the horizontal transect, the average facet diameter is approximately 60% larger in the adult (61.6 ± 4.5 µm) relative to the nymph (38.5 ± 2.0 µm). However, whereas in the nymph, the largest ommatidia are located at the eye equator and decrease in size in the dorsal and ventral directions, in the adult, ommatidial size increases from the equator towards the ventral region, reaching its maximum at the ventral-most region of the eye. These facet diameter profiles indicate that optical sensitivity peaks at the eye equator in the nymph, whereas in the adult, peak sensitivity shifts to the ventral-most region of the eye.

4. Discussion

Here, we have characterized the functional morphology of the compound eye of the kissing bug *R. prolixus* and the changes it experiences along ontogeny. These eyes are approximately hemispherical-shaped eyes which allow visual sampling of the whole surrounding space with the exception of the space region occupied by its own body (figures 1, 3). We have observed that in the adult stage, the eye experiences growth that exceeds the increment expected by extrapolating the growth rate across nymphal instars (figure 2). The size increment occurs in both the dorsoventral and anteroposterior perimeters of the eye (figure 2*E*,*H*, respectively), as well as in these perimeters normalized to head size (figure 2*F*,*I*). These increases in size are more pronounced in the anterior and ventral regions of the eye (figure 2*G*,*J*). Regarding eye spatial sampling frequency, we observed no substantial differences between the last nymphal instar and the adult stage, either along the eye equator or along the vertical transect in the lateral region of the eye (figure 4*C*,*E*). The only exception was a slight increase in sampling frequency in the ventral region of the adult eye. The ommatidial diameter, instead, was found to be considerably larger than expected in the adult stage (figure 2*M*). Along the eye equator, this parameter was rather constant in both the last nymphal instar and the adult stage (figure 4*D*). By contrast, along the vertical transect, ommatidial diameter reaches its maximum at the eye equator in the fifth-instar nymph, while in the adult stage the largest ommatidia are found in the ventral region (figure 4*F*). Thus, the area of highest sensitivity along

the vertical transect shifts from the equatorial region in the nymphal instar to the ventral region in the adult.

The apposition compound eye with fused rhabdoms is the ancestral eye design in insects. Open rhabdoms are a derived feature that has evolved not only in Heteroptera but also in three other insect orders (Dermaptera, Coleoptera and Diptera [30]). This arrangement of photoreceptor rhabdomeres enhances light sensitivity, typically at the expense of spatial acuity [28,30]. Ommatidia with open rhabdoms contain screening pigments that form a pupil whose aperture determines the angular extent of each ommatidium's field of view around its optical axis [31]. In dim light, the pupil opens, increasing the ommatidial field of view, whereas in bright light it closes, reducing it. When the pupil is open, all photoreceptors receive focused light; when it is closed, the peripheral photoreceptors (R1-6) are shielded by pupillary pigments. This arrangement provides a low-acuity scotopic system in which all eight photoreceptors are illuminated, and a high-acuity photopic system in which only the central photoreceptors (R7-8) receive light [30]. Accordingly, the interommatidial angles measured here provide an estimate of the upper limit of visual acuity that *R. prolixus* can achieve in bright light, whereas its acuity in dim light is expected to be lower.

Apposition eyes are typically associated with insects active during daylight hours, when the number of available photons is not a major limiting factor. However, some nocturnal insects have apposition eyes adapted for vision in dim light. They achieve this through one or a combination of the following adaptations: increasing the aperture through which light enters the ommatidium, increasing the combined acceptance angle of the rhabdomeres, or employing spatial and/or temporal summation mechanisms [32]. Here, we found that triatomines have compound eyes with remarkably large facet areas, which increase the amount of light entering each ommatidium, consistent with their crepuscular and nocturnal habits (figures 2*M* and 4*D*,*F*) [7,8]. When the diameters of these facets are compared with those of other insects with apposition compound eyes, it becomes clear that adult triatomine facet lenses are unusually large (70 µm in the ventral region of the *R. prolixus* eye; figure 4*F*). In most crepuscular and nocturnal insects with apposition eyes, facets are large, with maximum diameters ranging from 32 to 60 µm (the nocturnal mosquito *Anopheles gambiae*, 32 µm [33]; the nocturnal praying mantis *Tenodera australasiae*, 50 µm [34]; the nocturnal cockroach *Periplaneta americana*, 40 µm [35]; the nocturnal bee *Megalopta genalis*, 36 µm [36]; the crepuscular butterfly *Caligo memnon*, 48 µm [37]; the nocturnal bull ant *Myrmecia nigriceps*, 34 µm [38]; the cave-dwelling beetle *Zophobas morio*, 60 µm [39]). Larger facets, close to those of *R. prolixus*, have been reported only for a considerably larger insect: the crepuscular dragonfly *Zyxomma obtusum* (75 µm [40]).

Based on our observations in *R. prolixus*, we analysed how the compound eyes of other triatomine species are modified throughout ontogeny. We found that *R. prolixus* is not the only triatomine species that shows a considerable enlargement of the eyes in the adult stage. *T. infestans*, for example, also exhibits a significant enlargement of the eye, which is also more pronounced in the ventral region (supplementary material, figure S2). In addition, although we were unable to quantify the eye size of the nymphal and adult stages in insects of the genus *Panstrongylus*, bibliographic and online collections show that the nymphal instars of this genus possess small compound eyes, whereas adults possess large eyes [41,42]. Figure 5*A* presents photographs from different perspectives of the *Panstrongylus megistus* eye, illustrating the remarkable eye growth between the last nymphal instar and the adult stage. A particular condition regarding adult eye size is observed in animals from the genus *Mepraia*. In the last nymphal instar, animals possess relatively small eyes [41]; however, in the adult stage the presence of a large eye is contingent upon the presence of wings. Adult females of this genus are apterous (wingless) and possess relatively small compound eyes, whereas males typically develop wings and exhibit significantly larger eyes (figure 5*B*) [43]. Furthermore, in the species *Mepraia spinolai*, there are also apterous adult males. Interestingly, the eye size in these particular males is relatively small, as observed in females (figure 5*B*). In summary, animals of the genus *Mepraia* also exhibit eye enlargement in the adult stage, which is closely linked to wing development. Thus, in all specimens from the genera *Rhodnius*, *Triatoma*, *Panstrongylus* and *Mepraia* that we could analyse, the development of large compound eyes in the adult is tightly associated with the presence of wings.

In addition, in the adult eye of *R. prolixus*, we observed a considerable ventral enlargement compared to the eye of the last nymphal instar. Although in the adult stage, the eye grows in both dorsal and ventral directions, it extends ventrally until nearly contacting the contralateral eye at the head midline (figure 1*H*(vi)). Moreover, whereas the ommatidial size is dorsoventrally symmetrical in the last nymphal instar (light blue curve in figure 4*F*), in the adult, ommatidial size increases monotonically from the dorsal to the ventral region of the eye, where it reaches its maximum (red curve in figure 4*F*). Thus, in *R.*

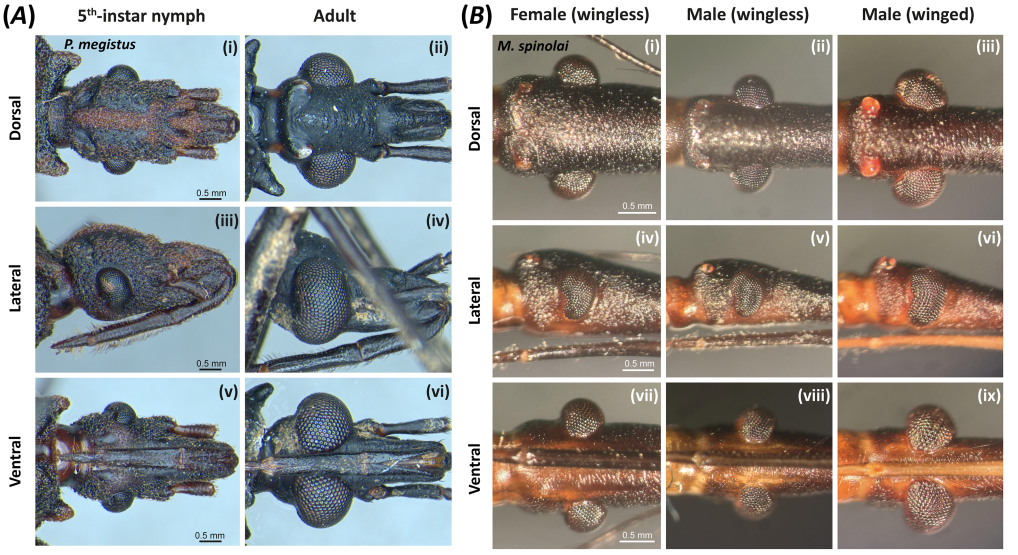

Figure 5. External morphology of the compound eyes of different triatomine species. (*A*) Different views of the heads of a fifth-instar nymph and an adult of *P. megistus*: (i–ii) dorsal; (iii–iv) lateral; (v–vi) ventral. (*B*) Different views of the heads of a wingless adult female, a wingless adult male and a winged adult male of *M. spinolai*: (i–iii) dorsal; (iv–vi) lateral; (vii–ix) ventral. Scale bars in panels (*A–B*) apply to all images within each respective row.

prolixus, the adult eye becomes asymmetrical in both eye shape and ommatidial size. We could directly confirm that the eye also transitions from being symmetrical in the last nymphal instar to asymmetrical in the adults of *T. infestans*, *P. megistus* and winged adult males of *M. spinolai* (supplementary material, figure S2; figure 5). Furthermore, we analysed the evidence available in the bibliography and in online collections to evaluate adult eye symmetry [41,42]. After visually inspecting 39 species from 10 genera, we observed that in 36 species from 9 genera, the adult eye possesses a greater ventral than dorsal extension and larger ommatidia in the ventral than in the dorsal region (supplementary material, table S3). Thus, an asymmetrical adult eye appears to be the most common eye pattern among triatomines.

As mentioned before, triatomines are obligate haematophagous insects that feed on warm-blooded hosts almost exclusively during the night. Throughout their lives, kissing bugs naturally seek to hide in folds or dark crevices that serve as shelters from which they perform foraging excursions. Olfactory and thermal cues have been considered the main sensory drivers of feeding behaviour [44]. A role of vision in this behaviour has been classically neglected (discussed in [17]). We have recently shown that vision in triatomines plays a clear role in supporting defensive behaviours. Directional escaping, freezing or combinations of these responses can be visually evoked in a fast and flexible manner according to the evaluation of the impending risk that the visual stimuli entail. Laterally placed eyes possessing a panoramic view of the world with a minimal posterior blind spot are characteristic of prey animals [45]. Such orientation of the eyes allows the insects to scan almost the 360° horizon around them, constantly on the lookout for potential threats, for example, during foraging excursions. Thus, the visual field outlined here for the *R. prolixus* eye is consistent with previous findings indicating a role of the visual system in supporting defensive behaviours [17].

Adult triatomines become exposed to predators not only during walking foraging excursions but also during dispersal and host-seeking flights. Therefore, the great enlargement of the eye in the adults could serve to better cope with the additional risk that flights entail. This hypothesis is supported by the fact that large eyes are found only in triatomines that possess wings. The ventral expansion of the eye in winged triatomines could be associated with the novel features of the aerial niche. By contrast to terrestrial locomotion, flight exposes triatomines to threats approaching from below. A more developed ventral region of the eye could better address the need for monitoring the space beneath the animal. Additionally, stimuli approaching from ventral directions may exhibit lower contrast against the ground than those approaching from above, which are typically silhouetted against the sky. Greater optical sensitivity increases the signal-to-noise ratio of photoreceptors and downstream neurons, thereby increasing the capacity to detect low-contrast stimuli [32,46]. This could explain why ventral ommatidia have approximately twice the area of the dorsal ones: their larger size provides greater light sensitivity and, thus, higher contrast sensitivity.

In addition to supporting defensive behaviours, vision has been shown to be involved in dispersal flights. Dispersal flights of triatomines generally occur in starving adults that do not have access to blood sources [11]. Under controlled laboratory settings, it was observed that take-off activity is oriented towards focal sources of light [13,47]. In the field, house lights and street lights, as well as traplights placed in different natural environments have been shown to attract dispersing triatomines (e.g. [14]). These directional light-sensitive behaviours may benefit significantly from a sensitive compound eye. Similarly, flight control could also benefit from it. Regarding the ventral development of the eye, it has been shown that visual motion flow in the ventral visual field of different insects can assist in controlling flight speed, altitude and landing manoeuvres (e.g. [48,49]). In addition, information on light polarization in this region of the visual field helps various insects orient their flight direction [50,51]. However, despite the epidemiological importance of triatomine dispersal and host-seeking flights, no studies characterizing these flights or their control have yet been conducted. The characterization of the compound eye outlined here provides a solid framework for testing specific hypotheses regarding the visual control of triatomine flight.

There is a clear relationship between the acquisition of flight and the development of compound eyes, both in holometabolous insects and in different morphs or phases of hemimetabolous insects. For instance, among holometabolous species, winged males and females of the ant *Camponotus pennsylvanicus*, which display nuptial flights, show significantly larger eyes and more ommatidia than workers of equivalent head size [52]. Among hemimetabolous species, for example, several differences in the compound eyes of the solitarious and gregarious locust phases have been reported, including opsin expression, eye size, ommatidial number and sensitivity to motion stimuli [53]. However, to our knowledge, no studies have reported an improvement in visual capabilities beyond expected by ontogeny when hemimetabolous insects develop wings at the imaginal molt. This gap may reflect either the absence of such a correlation in hemimetabolous insects—negative results tend to be underreported—or insufficient study of this relationship within the group. A systematic approach to testing this hypothesis would involve studying the post-embryonic eye development in hemimetabolous insect groups at increasing phylogenetic distance from triatomines.

Ethics. All the experimental protocols were performed in accordance with the relevant guidelines and ethical regulations of the Facultad de Ciencias Exactas y Naturales (Universidad de Buenos Aires).

Data accessibility. The data and code supporting this article are available at Zenodo [54].

Supplementary material is available online [55].

Declaration of AI use. Artificial intelligence tools (Claude, Anthropic) were used solely to assist with English language editing.

Authors' contributions. T.M.C.: conceptualization, data curation, formal analysis, investigation, methodology, software, visualization, writing—original draft; H.G.G.: resources; V.P-S.: formal analysis, methodology; S.A.M.: data curation, investigation, methodology, supervision, writing—review and editing; M.B.A.: conceptualization, data curation, formal analysis, funding acquisition, investigation, methodology, project administration, resources, supervision, writing—original draft.

All authors gave final approval for publication and agreed to be held accountable for the work performed therein.

Conflict of interest declaration. We declare we have no competing interests.

Funding. This study was supported by the Universidad de Buenos Aires (UBACYT 20020220100096BA to M.B.A.).

Acknowledgements. We are grateful to Javier Santos for kindly providing the chimeric TAT-GFP used for fluorescent pseudopupil contrast enhancement. We also thank Raquel Aparecida Ferreira, Frederico Dutra Kirst and the Coleção de Vetores de Tripanosomatídeos (Instituto René Rachou, Fundação Oswaldo Cruz) for sharing photographs of several species of the genera *Panstrongylus, Triatoma* and *Rhodnius* (the photographs of *P. megistus* were included in figure 5). We thank Carezza Botto-Mahan for her support in providing specimens of *M. spinolai* for photography and Pablo Schilman for granting us access to confocal microscope. Finally, we are grateful to Doekele Stavenga for his thorough insights regarding the visualization of the photoreceptors and the process of light adaptation in the ommatidia of *R. prolixus.*

References

1. Schofield CJ. 1988 The biosystematics of Triatominae. In *Biosystematics of haematophagous insects* (ed. MW Service), pp. 284–312. Oxford, UK: Clarendon Press.
2. World Health Organization. *Chagas disease (American trypanosomiasis)*. https://www.who.int/health-topics/chagas-disease}tab=tab_1.
3. Barrozo RB, Reisenman CE, Guerenstein P, Lazzari CR, Lorenzo MG. 2017 An inside look at the sensory biology of triatomines. *J. Insect. Physiol.* **97**, 3–19. (doi:10.1016/j.jinsphys.2016.11.003)

4. Alevi KCC, de Oliveira J, da Silva Rocha D, Galvão C. 2021 Trends in taxonomy of Chagas disease vectors (Hemiptera, Reduviidae, Triatominae): from Linnaean to integrative taxonomy. *Pathogens* **10**, 1627. (doi:10.3390/pathogens10121627)
5. Lent H, Wygodzinsky P. 1979 Revision of the Triatominae (Hemiptera, Reduviidae) and their significance as vectors of Chagas disease. *Bull. Am. Mus. Nat. Hist.* **163**, 125–520.
6. Abad-Franch F, Gurgel-Gonçalves R. 2021 The ecology and natural history of wild Triatominae in the Americas. In *Triatominae—the biology of Chagas disease vectors* (eds A Guarneri, M Lorenzo), pp. 387–445. Cham, Switzerland: Springer.
7. Constantinou C. 1984 Photoreceptors involved in the entrainment of the circadian activity rhythm of the blood-sucking bug, *Rhodnius pholixus*. *Biol. Rhythm Res.* **15**, 195–201. (doi:10.1080/09291018409359851)
8. Lazzari CR. 1992 Circadian organization of locomotion activity in the haematophagous bug *Triatoma infestans*. *J. Insect Physiol.* **38**, 895–903. (doi:10.1016/0022-1910(92)90101-I)
9. Barrozo RB, Schilman PE, Minoli SA, Lazzari CR. 2004 Daily rhythms in disease-vector insects. *Biol. Rhythm Res.* **35**, 79–92. (doi:10.1080/09291010412331313250)
10. Lazzari CR. 2021 The behaviour of kissing bugs. In *Triatominaethe: biology of Chagas disease vectors* (eds A Guarneri, M Lorenzo), pp. 215–238. Cham, Switzerland: Springer.
11. Lehane MJ, McEwen PK, Whitaker CJ, Schofield CJ. 1992 The role of temperature and nutritional status in flight initiation by *Triatoma infestans*. *Acta Trop.* **52**, 27–38. (doi:10.1016/0001-706x(92)90004-h)
12. Reisenman CE, Lazzari CR. 2006 Spectral sensitivity of the photonegative reaction of the blood-sucking bug *Triatoma infestans* (Heteroptera: Reduviidae). *J. Comp. Physiol. A.* **192**, 39–44. (doi:10.1007/s00359-005-0045-x)
13. Minoli SA, Lazzari CR. 2006 Take-off activity and orientation of triatomines (Heteroptera: Reduviidae) in relation to the presence of artificial lights. *Acta Trop.* **97**, 324–330. (doi:10.1016/j.actatropica.2005.12.005)
14. Pacheco-Tucuch FS, Ramirez-Sierra MJ, Gourbière S, Dumonteil E. 2012 Public street lights increase house infestation by the Chagas disease vector *Triatoma dimidiata*. *PLoS ONE* **7**, e36207. (doi:10.1371/journal.pone.0036207)
15. Nilsson DE. 2022 The evolution of visual roles—ancient vision versus object vision. *Front. Neuroanat.* **1**, 789375. (doi:10.3389/fnana.2022.789375)
16. Lazzari CR, Varjú D. 1990 Visual lateral fixation and tracking in the haematophagous bug *Triatoma infestans*. *J. Comp. Physiol. A.* **167**, 527–531. (doi:10.1007/BF00190823)
17. Chialina TM, Vidal BL, Minoli SA, Beron de Astrada M. 2025 Visually-guided defensive behaviors in triatomines (Heteroptera: Reduviidae). *J. Insect Physiol.* **165**, 104862. (doi:10.1016/j.jinsphys.2025.104862)
18. Reisenman CE, Insausti TC, Lazzari CR. 2002 Light-induced and circadian changes in the compound eye of the haematophagous bug *Triatoma infestans* (Hemiptera: Reduviidae). *J. Exp. Biol.* **205**, 201–210. (doi:10.1242/jeb.205.2.201)
19. Insausti TC, Le Gall M, Lazzari CR. 2013 Oxidative stress, photodamage and the role of screening pigments in insect eyes. *J. Exp. Biol.* **216**, 3200–3207. (doi:10.1242/jeb.082818)
20. Fischer C, Mahner M, Wachmann E. 2000 The rhabdom structure in the ommatidia of the Heteroptera (Insecta), and its phylogenetic significance. *Zoomorphology* **120**, 1–13. (doi:10.1007/s004359900018)
21. Settembrini BP. 1984 Circadian rhythms of locomotion activity in *Triatoma infestans* (Hemiptera: Reduviidae). *J. Med. Entomol.* **21**, 204–212. (doi:10.1093/jmedent/21.2.204)
22. von Müller J. 1970 Feinbau und Dunkelanpassung der Komplexaugen von (Stål). *Zool. Jahrb. Abt. allg. Zool. Physiol. Tiere* **75**, 111–133.
23. Dander U, Jander R. 1994 Numerical allometric growth of the ommatidia, antennal sensilla, and teeth of foretibial combs in the milkweed bug *Oncopeltus fasciatus* Dallas (Heteroptera: Lygaeidae). *Int. J. Insect Morphol. Embryol.* **23**, 329–344. (doi:10.1016/0020-7322(94)90029-9)
24. Schindelin J *et al.* 2012 Fiji: an open-source platform for biological-image analysis. *Nat. Methods* **9**, 676–682. (doi:10.1038/nmeth.2019)
25. Stavenga DG. 1979 Pseudopupils of compound eyes. In *Comparative physiology and evolution of vision in invertebrates* (ed. H Autrum), pp. 357–439. Berlin, Germany: Springer.
26. Gutiérrez D, Rigosi E, Nagloo N, O'Carroll D, Warrant EJ. 2024 Spatial resolution and optical sensitivity in the compound eyes of two common European wasps, *Vespula germanica* and *Vespula vulgaris*. *J. Exp. Biol.* **227**, jeb246670. (doi:10.1242/jeb.246670)
27. Berón de Astrada M, Bengochea M, Medan V, Tomsic D. 2012 Regionalization in the eye of the grapsid crab *Neohelice granulata* (= *Chasmagnathus granulatus*): variation of resolution and facet diameters. *J. Comp. Physiol. A* **198**, 173–180. (doi:10.1007/s00359-011-0697-7)
28. Land MF. 1997 Visual acuity in insects. *Annu. Rev. Entomol.* **42**, 147–177. (doi:10.1146/annurev.ento.42.1.147)
29. Franceschini N, Kirschfeld K, Minke B. 1981 Fluorescence of photoreceptor cells observed *in vivo*. *Science* **213**, 1264–1267. (doi:10.1126/science.7268434)
30. Osorio D. 2007 Spam and the evolution of the fly's eye. *BioEssays* **29**, 111–115. (doi:10.1002/bies.20533)
31. Nilsson DE, Ro AI. 1994 Did neural pooling for night vision lead to the evolution of neural superposition eyes? *J. Comp. Physiol. A* **175**, 289–302. (doi:10.1007/BF00192988)
32. Warrant EJ. 2017 The remarkable visual capacities of nocturnal insects: vision at the limits with small eyes and tiny brains. *Phil. Trans. R. Soc. B* **372**, 20160063. (doi:10.1098/rstb.2016.0063)
33. Land MF, Gibson G, Horwood J. 1997 Mosquito eye design: conical rhabdoms are matched to wide aperture lenses. *Proc. R. Soc. B* **264**, 1183–1187. (doi:10.1098/rspb.1997.0163)

34. Rossel S. 1979 Regional differences in photoreceptor performance in the eye of the praying mantis. *J. Comp. Physiol.* **131**, 95–112. (doi:10.1007/BF00619070)
35. Butler R. 1973 The anatomy of the compound eye of *Periplaneta americana* L.: 2. Fine structure. *J. Comp. Physiol.* **83**, 239–262. (doi:10.1007/BF00693677)
36. Greiner B, Ribi WA, Warrant EJ. 2004 Retinal and optical adaptations for nocturnal vision in the halictid bee *Megalopta genalis*. *Cell Tissue Res.* **316**, 377–390. (doi:10.1007/s00441-004-0883-9)
37. Frederiksen R, Warrant EJ. 2008 Visual sensitivity in the crepuscular owl butterfly *Caligo memnon* and the diurnal blue morpho *Morpho peleides* : a clue to explain the evolution of nocturnal apposition eyes? *J. Exp. Biol.* **211**, 844–851. (doi:10.1242/jeb.012179)
38. Narendra A, Reid SF, Greiner B, Peters RA, Hemmi JM, Ribi WA, Zeil J. 2011 Caste-specific visual adaptations to distinct daily activity schedules in Australian *Myrmecia* ants. *Proc. R. Soc. B* **278**, 1141–1149. (doi:10.1098/rspb.2010.1378)
39. Ro AI, Nilsson DE. 1993 Sensitivity and dynamics of the pupil mechanism in two tenebrionid beetles. *J. Comp. Physiol. A* **173**, 455–462. (doi:10.1007/BF00193518)
40. Horridge GA. 1978 The separation of visual axes in apposition compound eyes. *Phil. Trans. R. Soc. B* **285**, 1–59. (doi:10.1098/rstb.1978.0093)
41. Carcavallo RU, Galíndez-Girón I, Jurberg J, Lent H. 1998 *Atlas of Chagas' disease vectors in the Americas*. Rio de Janeiro, Brazil: Editora Fiocruz.
42. Faculdade de Ciências Farmacêuticas de Araraquara. 2026 *Coleção de Triatominae*. https://www2.fcfar.unesp.br/}!/triatominae/.
43. Hernández ML, Dujardin JP, Gorla DE, Catalá SS. 2015 Can body traits, other than wings, reflect the flight ability of Triatominae bugs? *Rev. Soc. Bras. Med. Trop.* **48**, 682–691. (doi:10.1590/0037-8682-0249-2015)
44. Guerenstein PG, Lazzari CR. 2009 Host-seeking: how triatomines acquire and make use of information to find blood. *Acta Trop.* **110**, 148–158. (doi:10.1016/j.actatropica.2008.09.019)
45. Hughes A. 1977 The topography of vision in mammals of contrasting life style. In *The visual system in vertebrates* (ed. F Crescitelli), pp. 613–756. Berlin, Germany: Springer.
46. Stöckl AL, Foster JJ. 2022 Night skies through animals' eyes—quantifying night-time visual scenes and light pollution as viewed by animals. *Front. Cell. Neurosci.* **16** 984282. (doi:10.3389/fncel.2022.984282)
47. Ortiz MI, Hincapié-Peñaloza E, Molina J. 2023 Electrophysiological detection of visible wavelengths of artificial lights indsucing take-off in adults of *Rhodnius prolixus* (Hemiptera: Triatominae). *Rev. Inst. Med. Trop. São Paulo* **65**, e25. (doi:10.1590/s1678-9946202365025)
48. Straw AD, Lee S, Dickinson MH. 2010 Visual control of altitude in flying *Drosophila*. *Curr. Biol.* **20**, 1550–1556. (doi:10.1016/j.cub.2010.07.025)
49. Linander N, Baird E, Dacke M. 2017 How bumblebees use lateral and ventral optic flow cues for position control in environments of different proximity. *J. Comp. Physiol. A* **203**, 343–351. (doi:10.1007/s00359-017-1173-9)
50. Heinloth T, Uhlhorn J, Wernet MF. 2018 Insect responses to linearly polarized reflections: orphan behaviors without neural circuits. *Front. Cell Neurosci.* **12**, 50. (doi:10.3389/fncel.2018.00050)
51. Meglič A, Ilić M, Pirih P, Škorjanc A, Wehling MF, Kreft M, Belušič G. 2019 Horsefly object-directed polarotaxis is mediated by a stochastically distributed ommatidial subtype in the ventral retina. *Proc. Natl Acad. Sci. USA* **116**, 21 843–21 853. (doi:10.1073/pnas.1910807116)
52. Klotz JH, Reid BL, Gordon WC. 1992 Variation of ommatidia number as a function of worker size in *Camponotus pennsylvanicus* (DeGeer) (Hymenoptera: Formicidae). *Insectes Soc.* **39**, 233–236. (doi:10.1007/BF01249297)
53. Schmeling F, Wakakuwa M, Tegtmeier J, Kinoshita M, Bockhorst T, Arikawa K, Homberg U. 2014 Opsin expression, physiological characterization and identification of photoreceptor cells in the dorsal rim area and main retina of the desert locust, *Schistocerca gregaria*. *J. Exp. Biol.* jeb.108514. (doi:10.1242/jeb.108514)
54. Chialina TM, Gentili HG, Pérez-Schuster V, Minoli SA, Beron de Astrada M. 2026 Data and code for: ontogenetic changes in eye morphology and sensitivity are associated with wing development in kissing bugs. Zenodo. (doi:10.5281/zenodo.20646553)
55. Chialina TM, Gentili HG, Pérez-Schuster V, Minoli SA, Beron de Astrada M. 2026 Supplementary material from: Ontogenetic changes in eye morphology and sensitivity are associated with wing development in kissing bugs. Figshare. (doi:10.6084/m9.figshare.c.8784975)